

A New Perspective and Explanation to the Formation of Plasmaspheric Shoulder Structure

Hua Zhang¹ Guangshai Peng¹ Chao Shen²

¹Institute of Space Weather, Nanjing University of Information Science & Technology, Nanjing, China.

²Harbin Institute of Technology, Shen Zhen, China.

Correspondence to: Hua Zhang (289534957@qq.com)

Abstract

Over the hours of 5-9 UT on June 8 2001, the extreme ultraviolet (EUV) instrument onboard IMAGE satellite observed a Shoulder-like formation in the morning sector and a Plume-like structure straddling in the between noon and dusk region. **The plasmopause formation is simulated using the Test Particle Model (TPM), based on drift motion, which reproduces various plasmopause structures and evolution of the Shoulder feature. The analysis indicates that the Shoulder is created by sharp reduction and spatial nonuniform of a dawn-dusk convection electric field intensity. Combined action of the plasmaspheric rotation rate speeding up with L-shell and plasma flux doing radial outflow in the predawn sector, results in an asymmetric bulge rotating eastward to reproduce the Shoulder structure.** The Shoulder structure rotates sunward and develops to the single or double Plume structure during an active times.

Keywords: plasmopause; shoulder-like; plume-like;IMAGE/EUV

1. Introduction

The plasmasphere is important region in the inner magnetosphere, surrounding the Earth and extending to 5 Earth radii(Re), which contains dense($10\text{-}10000\text{ cm}^{-3}$) and cold plasma (below 1ev). The plasmopause formed by a superposition of corotation and convection electric field in the inner magnetosphere (Nishida,1966; Chen and Wolf, 1972). The formation and size of plasmopause varies with geomagnetic activity level. Generally, as the disturbance level increasing, the plasmopause position closer

29 to the Earth and of shape deviate from circle in the equatorial plane (Grebowsky,
30 1970). Atypical plasmopause structures, such as ‘bulge’ and Plume occur often in both
31 whistler and in-situ data (Carpenter and Anderson,1992). There are many theoretical
32 researches study to explanation of the formation of Plume (Grebowsky,1970; Pierrard
33 and Lemaire, 2004; Zhang et al., 2013), and Pierrard and Cabrera (2006) firstly
34 simulated a double-Plumes , but not explained origin of second-Plume.

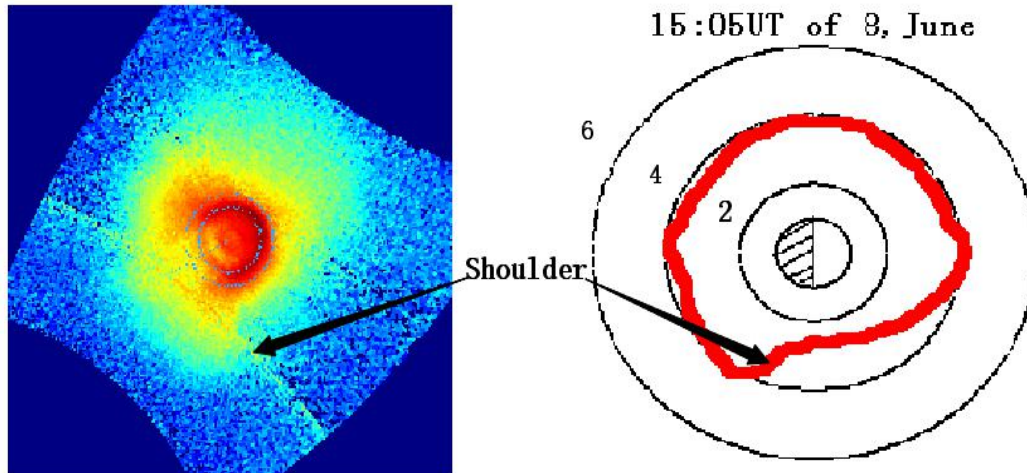
35 The EUV instrument onboard IMAGE satellite has launched in March, 2000,
36 which provided a global perspective to the plasmasphere, such as Plume, Finger,
37 Notch and Shoulder, and so on, some of plasmaspheric structures observed by EUV
38 (Sandel et al., 2001). One of plasmaspheric structures, Shoulder, has less study in the
39 previous papers than Plume. But, the Shoulder may play important role on a loss
40 mechanism for the ring current (Burch et al., 2001). So, it is important to study the
41 formation mechanism of Shoulder.

42 At present, there are no convincing explanations for dynamic formation of
43 Shoulder. Goldstein et al.(2002) firstly proposed an explanation, based on the
44 Magnetospheric Specification Model(MCM) simulation output, for the formation of
45 the Shoulder. They presented that the Shoulder is created by sudden decrease of
46 dusk-dawn electric field. As interplanetary magnetic field (IMF) turns northward
47 from southward, trigger antisunward flow of plasma in predawn sector, to produce
48 an asymmetric bulge called Shoulder. Later, based on physical mechanism of
49 interchange instability and a Kp-dependent E5D electric field model, Pierrard and
50 Lemaire (2004) suggested that the Shoulder is not the result of radial outflow of
51 plasma, same as the presentation of Goldstein et al. (2002) , but is inward plasma
52 drift in post-midnight sector.

53 Then, scarce papers about dynamical formation of the Shoulder are delivered than
54 of Plume. In this paper, we used TPM to simulate dynamical formation of the
55 Shoulder, using Weimer’s statistical E-field (Weimer, 2001; Zhang et al., 2012),
56 which is both spatially nonuniform and dynamically responsive to change
57 geomagnetic and solar wind conditions. To drive the TPM model, several inputs are
58 used: Dst; solar wind (SW) and interplanetary magnetic field (IMF) data sets. The

59 authors make attempt to a new convincing explanation for formation of the
60 Shoulder-like structure, different from the previous explanations.

61 2. Shoulder Observation



62
63 **Figure1. Snapshot of plasmasphere(left panel) by EUV instrument, at 15:05 UT of 8 June 2001,**
64 **Sunlight is incident from the upper right. Earth is in the center of panels and Shoulder is**
65 **observed and labeled in the snapshot. Right panel is plasmopause of that extracted from left**
66 **plasmapheric image.**

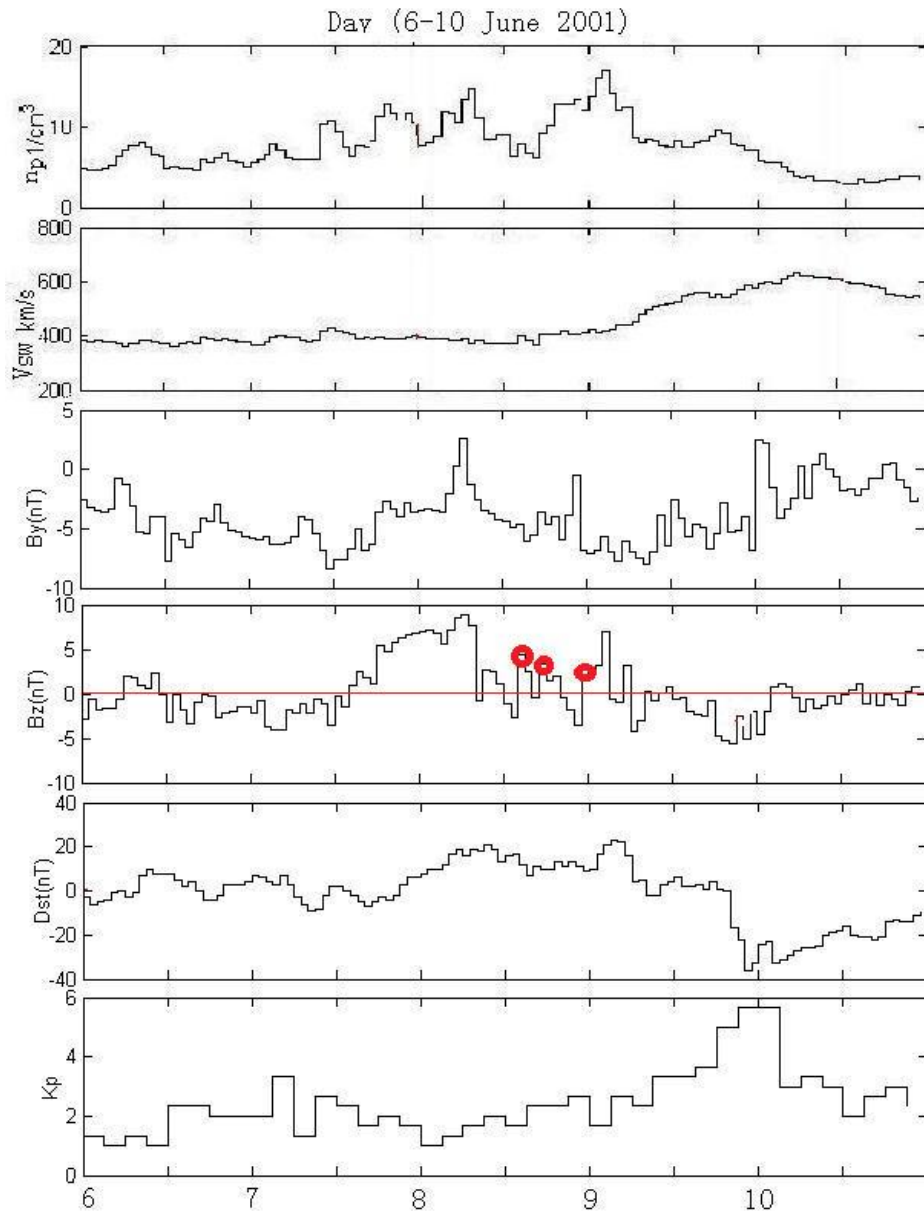
67 The Figure 1 illustrates the Shoulder-like structure, a sharp radial plasmaspheric
68 structure about 1 RE radial extension, in the post-midnight sector, which was viewed
69 by EUV imager onboard IMAGE satellite at 15.05 UT of 8 June 2001. The right panel
70 illustrates the plasmopause extracted from the left panel in the Figure1. The outer
71 boundary of plasmasphere is assumed to be 40% of maximum brightness of 30.4nm
72 He⁺ emission, where the intensity is the logarithm of the luminosity (Pierrard and
73 Cabrera, 2006). Then, the Shoulder-like is labeled and marked by arrows in the plot.
74 Comparison sequential observations with the simulation pictures, show that the
75 Shoulder structure keeping and corotating with the main plasmaspheric body can be
76 seen in Figure 3, and is discussed in the next section. That is mean the outer edge of
77 the Shoulder corotates faster than the inner edge in development phase (Goldstein et
78 al., 2002). Then, the Shoulder moves eastward to afternoon sector and evolves into
79 the Plume-like structure. Over the next hours, the outer body of Plume flows sunward
80 from noon sector, resulting in the Plume thinned out and disappeared (can see the

81 simulation of Figure 3). In the next section, we take the case of 8 June 2001
82 observation as an example, to discuss the simulation of the Shoulder and the Plume
83 evolution based on the TPM method.

84 **3. Simulation**

85 In region of plasmasphere occupied, charged particles are cold plasma (e.g. energy of
86 particles is $<1 \text{ eV}$). So, we can assume that plasma elements have only $\mathbf{E} \times \mathbf{B}/B^2$ drift
87 motions (Li and Xu, 2005; Lejosne and Mozer, 2016). Here, the electric field intensity
88 of E-model is superposition of convection and corotation electric field. Electric field
89 plays a key role on plasma drift motion and the formation of plasmasphere (Pierrard et
90 al., 2008). In the present paper, the Weimer's electric field (Weimer, 2001) is mapped
91 into the magnetosphere along magnetic lines to model the magnetospheric convection
92 electric field (Zhang et al., 2012), and T96 magnetic field to model the background
93 magnetic field.

94 In the simulation, the calculation regions is radial range of 2-7 R_e and azimuthal
95 span $0-359^\circ$. Dispersion by iso-spacing grids that correspond to the radial and
96 azimuthal steps are equal to $0.1R_e$ and 1° respectively, in the magnetic equatorial
97 plane. Ten particles are placed into each grid, so particle density is proportional to
98 L^{-1} which is not consistent with the actual density in a saturation state (close to true
99 density presumably is proportional to L^{-4}), but is adequate to study the evolution of
100 plasmaspheric morphology using a skeleton map of particles during a substorm period.
101 The TMP runs 3 days under the low activity condition to obtain the boundary conditions for
102 the simulation.



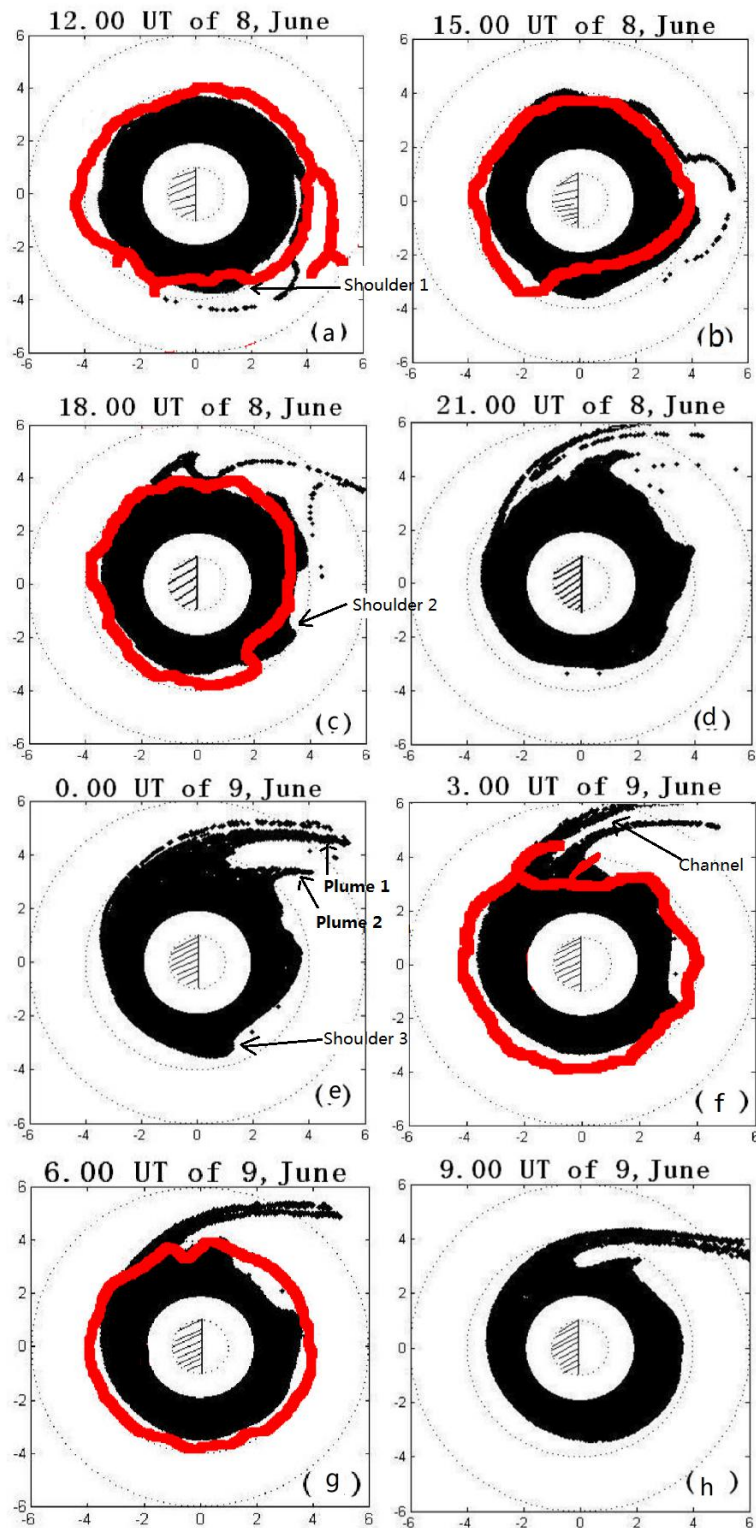
103

104 **Figure 2. Input parameters of TPM model, the variation of the By and Bz component of the IMF,**

105 **the Dst index and Kp index, on 6-10 June 2001, is a typical substorm case.**

106 The paper presents the case of 8-9 June 2001, to study the evolution of the
 107 shoulder and propose a hypothetical explanation produced by TPM simulation.
 108 During the geomagnetic substorm, all of the TPM inputs are available. IMF and
 109 Solar Wind data are available in ACE satellite data center, and Dst index can see
 110 in [World Data center for Geomagnetism, Kyoto](#). Fig.2 shows the By, Bz
 111 components of the IMF, the Dst index and the geomagnetic activity index Kp,
 112 observed over 6 to 10 June 2001. This is a typical substorm case that Kp index
 113 gradually increases up to 5+ and then decreases. The TPM runs with 3-minute

114 time resolution from 6 June at 00:00 UT to 10 June at 12:00 UT. The results of
115 simulation are showed in Fig.3, whose corresponding times are labeled on the title
116 of each panel. The simulation plasmapause is a skeleton which consists of
117 continuous particles distribution. Comparison of TPM simulation (black body)
118 and EUV observation (red line) in Fig.3, the simulated plasmopause positions
119 correspond generally rather favorable with the EUV observations. The results of
120 EUV observation show that the plasmopause is seldom smooth or irregular, due to
121 the fluctuations in plasmopause region cause by successive particles injection
122 during a disturbance period (Goldstein et al., 2002; Gallagher et al., 2005), in
123 agreement with previous whistler observations (Carpenter and Anderson,1992).
124 Contrary, The simulation of plasmapauses by TPM is better smooth. So,
125 observations and simulations are not identical, due to deviation in the extraction of
126 the boundary from EUV image and optical contamination of the image (Sandel et
127 al., 2001; Zhang et al., 2013) and the limitation in the TPM model and the
128 unrealistic Weimer electric field model. .



129

130 Figure 3. The simulation of plasmaspheric morphology compare with EUV/IMAGE observation in the
 131 geomagnetic equatorial plane on 8 - 9 June 2001. The red irregular curves indicate the plasmopause
 132 observation by EUV/IMAGE. Black contours are the plasmasphere simulated by TPM model. White
 133 contours are main plasmasphere (located at 1-2 Re region).The dotted circles on the panels correspond

134 to L=1, 2, 4 and 6.

135 Panels of Fig.3(a) - (h) illustrate the plasmasphere obtained on the interval of from
136 8 June at 12:00 UT to 9 June at 09:00 UT 2001, and every three hours output a
137 snapshot. The results of the simulation show that the evolution and development of
138 the features of the plasmopause, like Shoulders and Plumes. **One can see that the**
139 **plasmopause is closer to the Earth in the predawn sector.** The reason is the increase of
140 rotation velocity resulting in plasmopause of **inward flow** in the predawn sector
141 (Pierrard and Cabrera, 2006; Verbanac et al., 2018). At 15.05 UT of 8 June, the TPM
142 simulation captures a infant Shoulder-like structure in panel Fig.3 (b), and then
143 corotates with the plasmasphere body moved eastward and further reproduces a
144 mature Shoulder formation in Fig.3(c). The overall agreement between TPM
145 simulation and EUV observed is quite well, but the TPM Shoulder is located ~1.5
146 hours earlier in magnetic local time (MLT) that probably originated from the
147 convection electric field model (Goldstein et al., 2002; Pierrard and Cabrera, 2005;
148 Zhang et al., 2013).

149 The EUV observation illustrated in Fig.3 (f) shows that a Plume is indeed observed
150 in the afternoon or dusk sector. The results of the simulation also reproduce the
151 formation and the **evolution** of the Plumes, which derives from the Shoulder structure
152 **in this case**, illustrated in panels of Fig.3 (d)-(f). The simulation show that the
153 Shoulders generate in the post-midnight sector (Verbanac et al., 2018), and then
154 rotates eastward around the Earth to the afternoon sector (Goldstein et al., 2002).
155 When the level of geomagnetic activity increase, the plasma element in the Shoulder
156 around the outer plasmasphere would convection outward and then into the dayside
157 magnetopause (Li and Xu, 2005; Pierrard et al., 2008), and produce the plasmaspheric
158 Plume structure. **The Shoulder1 firstly arises on Fig.3(a) in the morning sector (at 12**
159 **UT, 8 June 2001), and then corotates with the main body of the plasmasphere to the**
160 **afternoon sector on Fig.3(c)(at 18 UT, 8 June 2001). During this period, Kp index**
161 **increases to 3+ from 1 (see in Fig.2), and magnetosphere convection slightly enhance**
162 **that triggers plasma elements in the Shoulder1 doing sunward convection, then**
163 **produces the Plume1 at 21 UT on 8 June 2001 (see in Fig.3(d)). The mature**

164 Shoulder2, illustrated in Fig.3(b), corotates eastward with the Earth to the
165 afternoon-dusk sector. During period of 0-3 UT on June 9, Kp index gradually
166 increases up to 5+, indicating that magnetospheric convection is enhanced and the
167 convective electric field increases. The infantile Plume2, illustrated in the panel of
168 Fig.3(e), derives from outflow of plasma elements in the Shoulder2, and evolves into
169 the mature Plume2 in Fig.3(f). Later, the double-plumes formation that is extension
170 from the plasmopause to the magnetosphere, presented in the simulation results in
171 panels of Figs.3 (e)-(f).

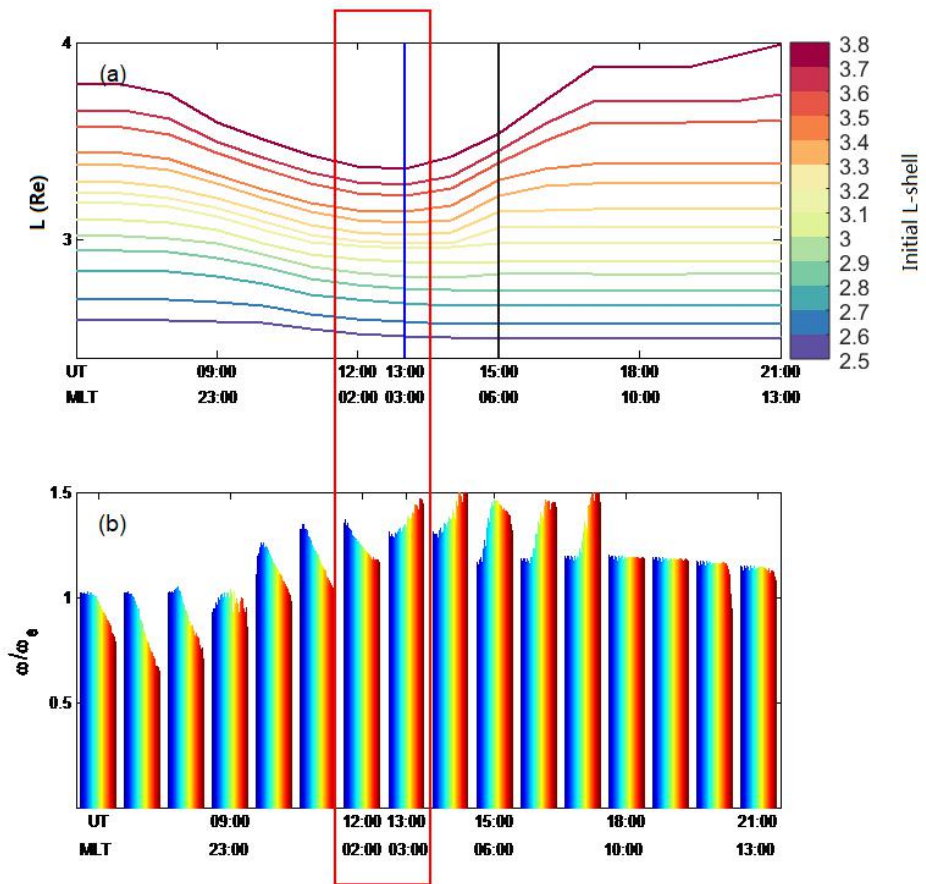
172 The cavity in between the double Plumes, or between Plumes and the main body
173 of plasmasphere, may be responsible for the formation of Channel and Notch
174 structures (Gallagher et al., 2005). The base and the westward edge of the Plume is
175 connected with the main body of plasmasphere. And there is a cavity topology, a
176 low-density region, between the tail structure of the plasmasphere and the main body
177 of plasmasphere. That is the channel structure of the plasmasphere. The Plume
178 corotates with the Earth to become thinner, and disappear finally (Li and Xu, 2005).
179 **The results of simulation reproduces the Channel structure in Fig.3(f).** Gallagher et al.
180 (2005) proposes that Notches and Channels share same origin, which derive from a
181 low-density cavity in the dusk region during recovery at the base of the plasmaspheric
182 Plume. The absence of Notch structure in this simulation event, **due to the fact that the**
183 **potential structure not cause the inward flow of plasma in the afternoon sector, and the**
184 **low disturbance time is maintaining for not long enough.**

185 By contrastive analysis on between Fig.2 and Fig.3, the formation of the
186 Shoulder is produced during the intensity of the convection electric field sudden
187 decrease (Goldstein et al., 2002; Pierrard and Lemaire, 2004), when IMF **sudden** turns
188 northward **from southward**. There are three Shoulders **reproduced** during this
189 substorm period, depicted in panels of Fig.3 (b)-(g). The time of the Shoulder
190 appearance are labeled by three red circles in Fig.2, at 14:00 UT, 17:00 UT, 23:00 UT
191 on 8 June respectively. At moment, the Bz component of the IMF turns northward.
192 But, not all of the times **of** the Bz component of the IMF turns northward, could
193 produce the Shoulder structure. **One can see that no shoulders reproduced in the**

194 results of the simulation, at 02:00 UT, 05:00 UT, and 08:00 UT on 9 June 2001
195 respectively. The Bz value of southward component must less than previous 24-hours
196 mean value. The intensity of the convection electric field is greater than previous
197 24-hours level. So the last closed equipotential line (LCE) would closer to the Earth
198 and results in plasmopause of inward flow in the predawn sector (Zhang et al., 2013).

199 **4. Discussion**

200 The physical explanation of Shoulder formation is not yet understood. In present
201 section, we use the case of Figure 1 as an example to investigate the physical
202 mechanism of Shoulder formation based on the TPM model. Fourteen test particles
203 are placed in the range of $2.5 \leq L \leq 3.8$, initial position locate at 12:00 MLT, space step
204 takes $0.1R_e$, and then trace these particles motion. Outputs are the trajectory (see in
205 Fig.4(a)) and the rotation rate (see in Fig.4(b)) of these test particles corresponding to
206 **both** given magnetic local time and universal time illustrated in the bottom of Fig.4.



207

208 Figure 4. The trajectory (upper plot) and the rotation rate (bottom plot) of 14 test particles
 209 corresponding to both UT (time -dependent) and MLT (location-dependent) during a substorm. The
 210 legend indicates fourteen test particles of various initial L-shell. The day is 8 June 2001.

211 The top panel shows that the outer part of plasmasphere ($L > 3.3$ Re) drift inward in
 212 the before 02:00 MLT sector, and move outward (could reach up to 3.9 Re position) in
 213 the predawn sector (after 03:00 MLT sector) (Verbanac et al., 2018). The radial motion
 214 of inner plasmasphere ($L < 3.3$) is negligible. The shoulder forming across a at
 215 03:00-06:00 MLT region (between blue vertical line and black vertical line in Figure
 216 4(a)). The outermost particle move outward 0.7 Re, and the fourth particle move
 217 outward 0.45 Re, from 03:00 MLT to 08:00 MLT. So, the Shoulder has a sharp eastern
 218 edge about $0.2\text{Re} \sim 0.3\text{Re}$ in radial extension and across a narrow 3-5 hours MLT
 219 region. Goldstein et al.(2002) proposed the shoulder formation by an outward radial

220 motion of plasma in a narrow range and in the morning sector. The conclusions of
221 Goldstein (2002) and Verbanac (2018) verify the simulation of this paper.

222 The lower panel shows the corotational angular velocity of test particles in the
223 range of $2.5 < L < 4.0$. The simulation results suggest that plasma element in
224 plasmasphere region rotation speed varies significantly with radial distance (Galvan,
225 2010). The inner part of plasmasphere rotates faster than its outer part in before 02:00
226 MLT sector, vice versa in a range of in the 03:00-08:00 MLT sector [Lejosne and
227 Mozer, 2016]. **The previous researchers analyzed the EUV observation and proposed**
228 **the Shoulder structure has MLT sharpening in the angular direction. It indicates that**
229 **the outer edge of the Shoulder rotates faster than the inner edge, resulting in**
230 **steepening of the MLT-profile of the Shoulder** (Goldstein et al., 2002). The lower
231 panel shows, with the increase of L, the rotation rate of the plasmasphere tends to
232 slightly decrease on the dusk side and obviously increase on the dawn side.

233 Fig. 4 indicates, in the region of 21:00 - 23:00:00 MLT, that the rotation rate is
234 about corotation in the inner plasmasphere ($L < 3$), but is the interval of 70% - 90% of
235 corotation in the outer plasmasphere ($L > 3$). The rotational value decreases with the
236 increase of L [Galvan et al., 2010]. Gallagher et al. (2005) investigates the drift rate of
237 notches in the geomagnetic quiet phase, and the results show that the average rotation
238 rate of plasmasphere is about 90% of the corotational rate, in agreement with the
239 results of Lejosne and Mozer (2016). When the plasma elements rotate to the region
240 of 23:00 - 02:00 MLT, rotation rate in the outer plasmasphere reaches to $\sim 130\%$ of
241 corotation, and in the inner plasmasphere is also close to the corotation rate. The
242 results show that the rotation rate of plasmasphere is overall increasing in the region.
243 In addition, the plasma elements in the outer plasmasphere rotate faster than the inner
244 plasmasphere in this region. The Fig.4(b) shows that rotation rate in the outer
245 plasmasphere highly reaches to $\sim 140\%$ of corotation, and rotation rate in the inner
246 plasmasphere is close to 110% of corotation. **So, we propose that the physical**
247 **mechanism of the shoulder formation is plasma extrusion of outer plasmasphere in the**
248 **predawn sector, due to outer plasmasphere both drifts radial outward and rotates faster.**
249 In present paper, the results show that the rotation rates of simulation are higher than

250 the observations, and not consistence with Huang et al. (2011) and Galvan et al.
251 (2010). The first reason is that this is a substorm case, so the convection of
252 magnetosphere is greater than the previous study articles of the geomagnetic quiet
253 case. (Galvan et al., 2010; Huang et al., 2011 ; Verbanac et al., 2018). And the second
254 reason is that the Weimer electric field model is larger in practice, which results in a
255 larger total electric field value in calculation (Goldstein et al., 2002; Pierrard et al.,
256 2008).

257 The dawn-dusk asymmetry of convective electric field is caused by the terminal
258 conductivity gradient of the ionosphere. The subrotation of the ionosphere drives the
259 subrotation of the plasmasphere, and the plasmaspheric drift is correlated with the
260 phase of geomagnetic storm (Burch et al., 2004). The convection electric field of
261 Weimer (2001) is obvious dawn-dusk asymmetry, that causes a smaller increase on
262 the dawnside and a lager decrease on the duskside, indicating that the subrotational
263 effect of the plasmasphere is modulated by field-aligned current changes and
264 conductance variations (Liemohn et al., 2004). The asymmetry of potential pattern
265 causes the sunward convection in the magnetospheric night-side to be larger than that
266 in the morning side, resulting in the subcorotational flow in the dark side. (Gallagher
267 et al., 2005).

268

269 **5. Conclusion**

270 In this paper, we have simulated the case of substorm on 8 June 2001 to investigate
271 the physical mechanism of the Shoulder formation based on TPM model that utilizes
272 Weimer's electric field and the drift motion theory. We use the E-model and the
273 B-model are quasi-static background field and global averages. So, the results of
274 simulation have some deviations with EUV observation. But, we have satisfactorily
275 reproduced the evolution and development of the features of the plasmopause, like the
276 Shoulders and Plumes. And then, the physical mechanism of the Shoulder formation
277 has been investigated.

278 The formation of Shoulder is association with IMF northward turning in the

279 predawn sector. And the physical mechanism of Shoulder formation is the result of
280 plasma extrusion in the predawn sector, caused by outer plasmasphere drifts radial
281 outward and rotates faster. Reversal of corotation rate with L-shell in post-midnight
282 sector compares with corotation rate in midnight sector. So, the shoulder forming
283 across a at 03:00-06:00 MLT region.

284 The formation and evolution of Plume and Channel have also been reproduce in
285 this case. One can see single or double Plumes appear in the dusk or afternoon sector,
286 and then become thinner with time, finally disappear.

287 At this model, we not consider the refilling process of ionosphere. In the future
288 work, the refilling process should be considered, expect to obtain more perfect results
289 comparing with EUV observations. And also, the physical mechanisms of
290 plasmaspheric features observed by EUV/IMAGE, like Notch or Channel, also are to
291 investigate by TPM model in future work underway.

292 **Author contributions:** Zhang H. conceptualized the project and wrote the original
293 draft of the paper. Peng G. S. modified the Figures and coded Fortran program. Shen C.
294 supervised the project, and reviewed and edited the paper.

295

296 **Acknowledgment:** The author thanks the professor D. R. Weimer, who provided the
297 code of Weimer's electric field model and ACE satellite data center and Word Data
298 center for Geomagnetism, Kyoto provided observation data. The dataset of
299 EUV/IMAGE could download from website <http://euv.lpl.arizona.edu/euv>.

300

301 **References**

302 Burch, J. L., Mende, S. B., Mitchell, D. G., Moore, T. E. , Pollock, C. J., Reinisch, B.
303 W., Sandel, B. R., Fuselier, S. A. , and Gallagher D. L.: Views of Earth's
304 magnetosphere with the IMAGE satellite, Science, 291, 691-624, doi:
305 10.1126/science.291.5504.619, 2001.

306 Carpenter, D. L. and Anderson, R. R.: An ISEE/Whistler model of equatorial
307 electron density in the magnetosphere, J. Geophys. Res., 97, 1097-1108,
308 doi:10.1029/91JA015481992, 1992.

309 Chen, A. J. and Wolf, R.A. : Effects on the plasmasphere of a time-varying convection
310 electric field, Planet. Space Sci., 20, 483-509, doi: 10.1016/0032-0633(72)90080-3,
311 1972.

312 Gallagher, D. L., Adrian, M. L. and Liemohn, M. W.: Origin and evolution of deep
313 plasmaspheric notches, J. Geophys. Res., 110, A09201, doi:10.1029/2004JA010906,
314 2005.

315 Galvan, D. A., Moldwin, M. B., Sandel, B. R., and Crowley, G. : On the cause of
316 plasmaspheric rotation variability: IMAGE EUV observation, J. Geophys. Res., 115,
317 A01214, doi:10.1029/ 2009JA014321, 2010.

318 Goldstein, J., Spiro, R. W., Reiff, P. H., Wolf, R. A., Sandel, B. R., Freeman, J. W., and
319 Lambour, R. L.: IMF-driven overshielding electric field and the origin of the
320 plasmaspheric shoulder of May 24, 2000, Geophys. Res. Lett., 29(16), 1819,
321 doi:10.1029/2001GL014534, 2002.

322 Grebowsky, J. M.: Model study of plasmopause motion, J. Geophys. Res., 75,
323 4329-4333, doi:10.1029/JA075i022p04329, 1970.

324 Huang Y., Xu, R. L., Shen, C., and Zhao H.: Rotation of the Earth's plasmasphere at
325 different radial distances, Adv. Space. Res., 48, 1167-1171, doi:
326 10.1016/j.asr.2011.05.028, 2011.

327 Lejosne, S., and Mozer, F. S. : Van Allen Probe measurements of the electric drift
328 $E \times B / B^2$ at Arecibo's L=1.4 field line coordinate, Geophys. Res. Lett., 43, 6768-6774,
329 doi: 10.1002/2016GL069875, 2016.

330 Li, L., and Xu, R. L.: Model of the evolution of the plasmasphere during a
331 geomagnetic storm, Adv. Space. Res., 36, 1895-1899. doi: 10.1016/j.asr.2003.10.057,
332 2005.

333 Nishida A.: Formation of plasmopause, or magnetospheric plasma knee, by the
334 combined action of magnetospheric convection and plasma escape from the tail, J.
335 Geophys. Res., 71, 5669-5679, doi:10.1029/JZ071i023p05669, 1966.

336 Pierrard V., and Lemaire, J. F.: Development of shoulders and plumes in the frame of
337 the interchange instability mechanism for plasmopause formation, Geophys. Res. Lett.,
338 31, L05809, doi:10.1029/2003GL018919, 2004.

339 Pierrard, V., and Cabrera, J.: Comparisons between EUV/IMAGE observations and
340 numerical simulations of the plasmopause formation, *Annales Geophysicae*, 23,
341 2635-2646, doi:10.5194/angeo-23-2635-2005, 2005.

342 Pierrard, V., and Cabrera, J.: Dynamical simulations of plasmopause deformations,
343 *Space.Sci.Res*, 122, 119-126, doi: 10.1007/s11214-006-5670-3, 2006.

344 Pierrard, V., Khazanov, G. V., Cebreira, J., and Lemaire, J.: Influence of the convection
345 electric field models on predicted plasmopause positions during magnetic storms. *J.*
346 *Geophys. Res.* 113, A08212, doi:10.1029/2007JA012612, 2008.

347 Sandel, B. R., King, R. A., Forrester, W. T., Gallagher, D. L., Broadfoot, A. L., and
348 Curtis, C. C.: Initial results from the IMAGE extreme ultraviolet imager, *Geophys.*
349 *Res. Lett.*, 28, 1439, doi: 10.1029/2001GL012885, 2001.

350 Verbanac, G., Bandic, M., Pierrard, V., and Cho, J.: MLT plasmopause characteristics:
351 Comparison between THEMIS observations and numerical simulations. *J. Geophys.*
352 *Res: Space physics*, 123, 2000-2007, doi:10.1002/2017JA024573, 2018.

353 Weimer, D. R.: An improved model of ionospheric electric potentials including
354 substorm perturbations and application to the Geospace Environment Modeling
355 November 24, 1996, event., *J. Geophys. Res.*, 106, 407-416,
356 doi:10.1029/2000JA000604, 2001.

357 Zhang, H., Xu, R. L., Zhao, H., and Shen, C.: The characteristics of the model of
358 Weimer's electric field within the magnetosphere., *Chinese J. Geophys.* 55, 36-45, doi:
359 10.6038/j.isnn.0001-5733.2012.01.004, 2012.

360 Zhang, H., Xu, R. L., Shen, C., and Zhao, H.: The simulation of the plasmaspheric
361 morphology during a magnetospheric disturbance event, *Chin J. Geophys*, 56,
362 731-737, doi:10.6038/cjg 20130302, 2013.